GODDARD GRANT
IN-37-CR
25831
P-33

FINAL TECHNICAL REPORT

INVESTIGATION OF AXIAL POSITIONING FOR FLEXURAL COMPRESSORS

Period Covered: 1 December 1988 - 31 July 1990

Grant NAG 5-1038

(NASA-CR-185711) INVESTIGATION OF AXIAL POSITIONING FOR FLEXURAL COMPRESSORS Final Technical Report, 1 Dec. 1988 - 31 Jul. 1990 (Washington Univ.) 33 p CSCL 13I

N91-26544

Unclas
G3/37 0025831

10 July 1991

Peter Riggle, Principal Investigator
Daniel B. Olsen, Project Engineer

TRI-CITIES UNIVERSITY CENTER
UNIVERSITY OF WASHINGTON
100 Sprout Road
Richland WA 99352

Prepared for NASA GODDARD SPACE FLIGHT CENTER, Greenbelt MD 20771

1.0 INTRODUCTION

This is the Final Technical Report for NASA Grant NAG 5-1038. The research performed under this grant can be divided into flexural bearing research, which was conducted under the original grant, and research into axial positioning of the armature in cryocooler compressors employing flexural bearings, which was performed under an extension to the original grant. The semi-annual report, which can be seen in Appendix A, focuses on flexure research and the analysis, design, and fabrication of the research compressor. This report focuses on the testing of the research compressor.

2.0 TESTING OF THE RESEARCH COMPRESSOR

The research compressor was assembled and disassembled repeatedly in order to show the consistency in which the piston and rod could be aligned with a .0004 inch radial gap around the piston. A full set of tests was completed for the first assembly which will be referred to as assembly #1. The compressor was disassembled and assembled a second time (assembly #2). Time did not permit assembly #2 to be fully tested. It was only tested statically.

2.1 Static Testing

Three types of static tests were done on the compressor to measure the spring constant of the flexures, the flux density in the air gap and the motor coefficient. Also a static test was done to characterize the clearance seal.

2.1.1 Spring Constant

The axial spring constant of the flexures was determined by applying pressure to the top of the piston and then measuring the deflection. A plot of force versus piston position is shown in Figure 1. The spring constant is linear for small displacements, but becomes nonlinear for larger displacements. The measured spring constant for the lower linear portion of the graph is

$$K = 29.0\ lb_f/in \quad \text{(measured)}$$

An analytical axial spring constant was calculated using a formula based on finite element analysis done during the first portion of this grant. The analytical value is

$$K = 26.4\ lb_f/in \quad \text{(analytical)}$$

2.1.2 Magnetic Field Measurement

The magnetic field was measured by running direct current through the motor coil and measuring the displacement. Since the spring constant is known, the force can be determined. A discontinuous linear spring constant is used to calculate the force. A plot of magnetic force versus current through the motor coil is shown in Figure 2. With this plot, one can calculate the motor coefficient ($\psi = F/i$) and the effective flux density (B) using the relation:

$$F = Bli$$

where F ≡ Applied magnetic force
l ≡ Effective coil wire length
i ≡ Motor coil current

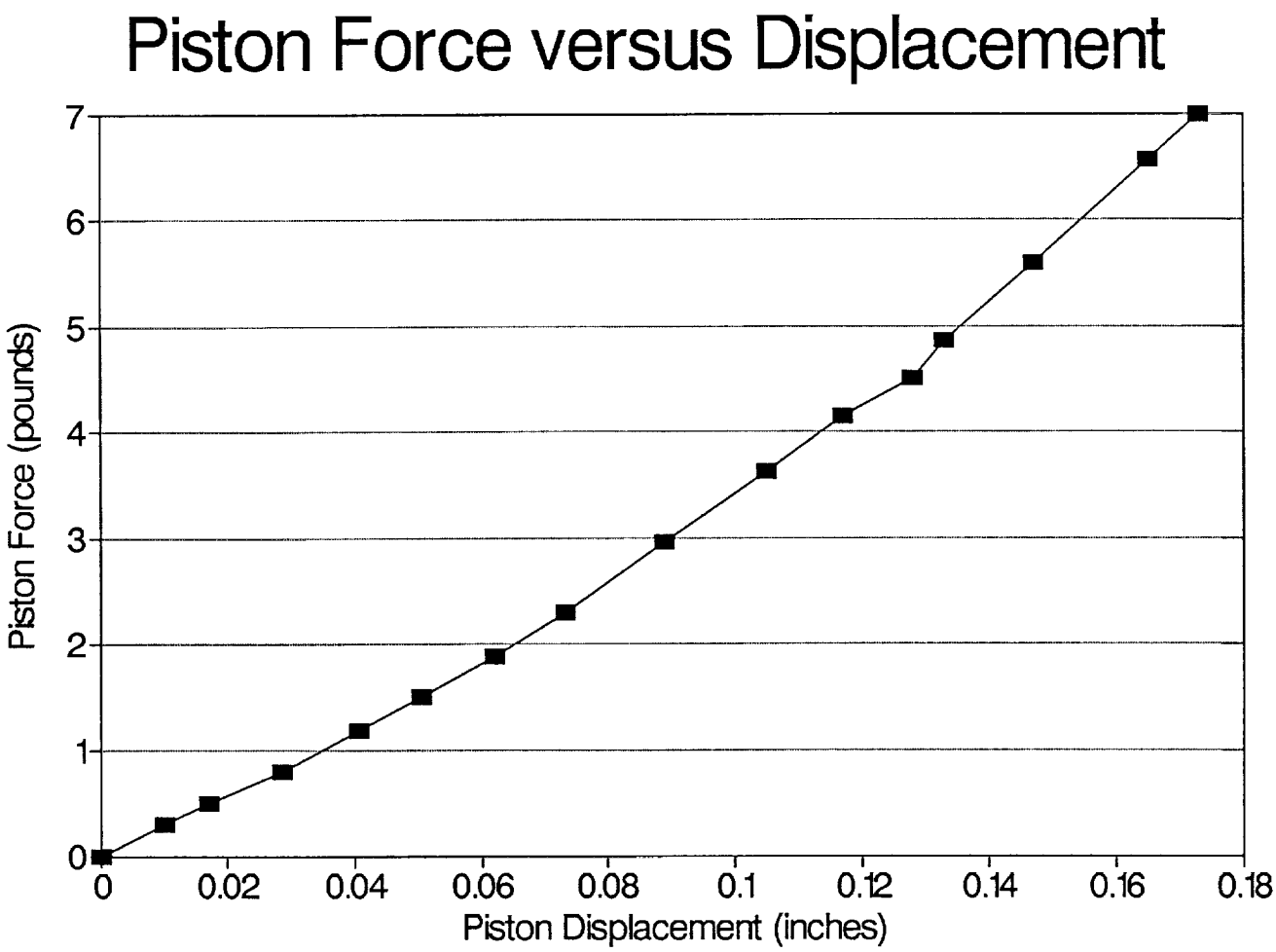

Figure 1. Pressure Force Versus Piston Position

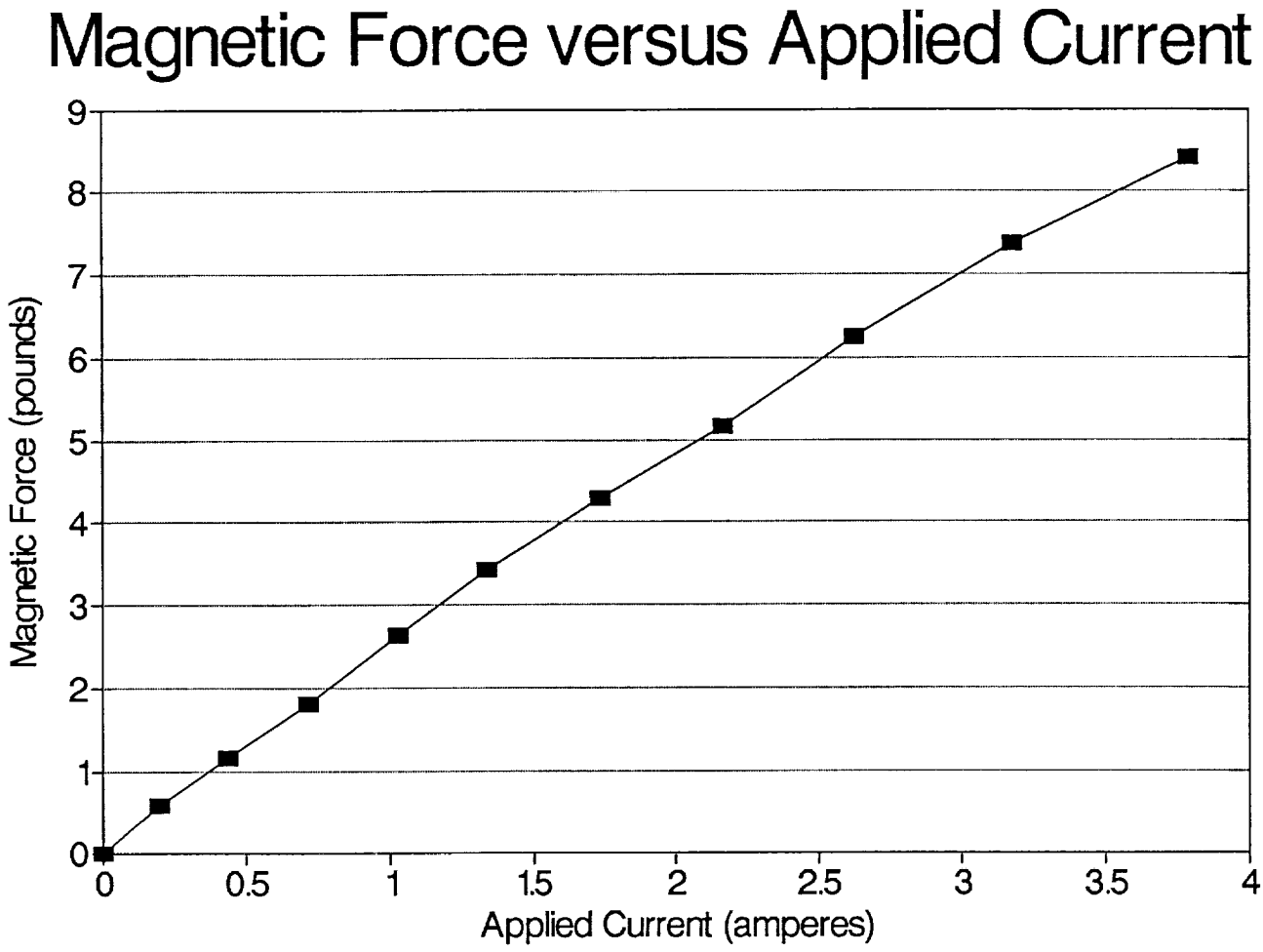

Figure 2. Magnetic Force Versus Motor Coil Current

The measured effective flux density and the motor coefficient for assembly #2 are

$$B = 10.4 \text{ KGauss}$$
$$\psi = 2.35 \text{ lb}_f/\text{ampere}$$

Assembly #2 used a ferromagnetic material for the piston rod to get higher strength for the rod. The result was a slight decrease in flux density from 10.7 KGauss to 10.4 KGauss. Cold rolled 302B stainless steel will be used for future rods.

2.1.3 Clearance Seal Characterization

The test done to characterize the clearance seal made it possible to compare the effectiveness of the seal from one assembly to another. It is a test of relative eccentricity of the piston from one assembly to the next. To test the clearance seal, the top of the piston (the side facing the compression space) was pressurized with air using a pressure regulator so that the piston was held at full stroke. The flow through the pressure regulator was then cut off and piston position and time values were recorded. The plot of position versus time is very close to being exponential, so a time constant can be calculated, which gives a measure of how good the clearance seal is. The time constants for both assemblies are

$$\tau = 13.0 \text{ seconds} \quad \text{(assembly \#1)}$$
$$\tau = 6.73 \text{ seconds} \quad \text{(assembly \#2)}$$

The larger the time constant the better the seal and the more concentric the piston is. We did have some rubbing problems with assembly #1, which might explain the fact that the assembly #1 time constant is larger than the assembly #2 time constant. A new piston was made for the second assembly using a larger clearance seal, designed to be the right clearance at operating temperature instead of at room temperature. The power loss due to the rub was quantified and determined to be insignificant. The problems which caused the rub were determined and the proper corrections were made for assembly #2. There was no detectable rub on assembly #2.

2.2 Dynamic Testing

Dynamic tests were run to determine the efficiency of the compressor at the design point, which is f = 40 Hz, P_{out} = 20 Watts, stroke = .394 in., and P_0 = 174 psi. Dynamic tests were run to determine the effect of the output power on efficiency. Dynamic tests were also run to quantify the axial decentering force and to gain insight into what causes the decentering force.

2.2.1 Experimental Test Set-up

The research compressor was loaded by a pneumatic resistance and two volumetric compliances. The pneumatic circuit is shown in Figure 3. The load on the compressor can be expressed as a complex number. The real part of the load is due to the pneumatic resistance. The imaginary part of the load is due to the force from the compliances of the gas spring and the flexures, and the inertial force of the moving mass. The compressor is most efficient when the imaginary part of the load is zero. Experimentally the imaginary part of the load was reduced to zero by

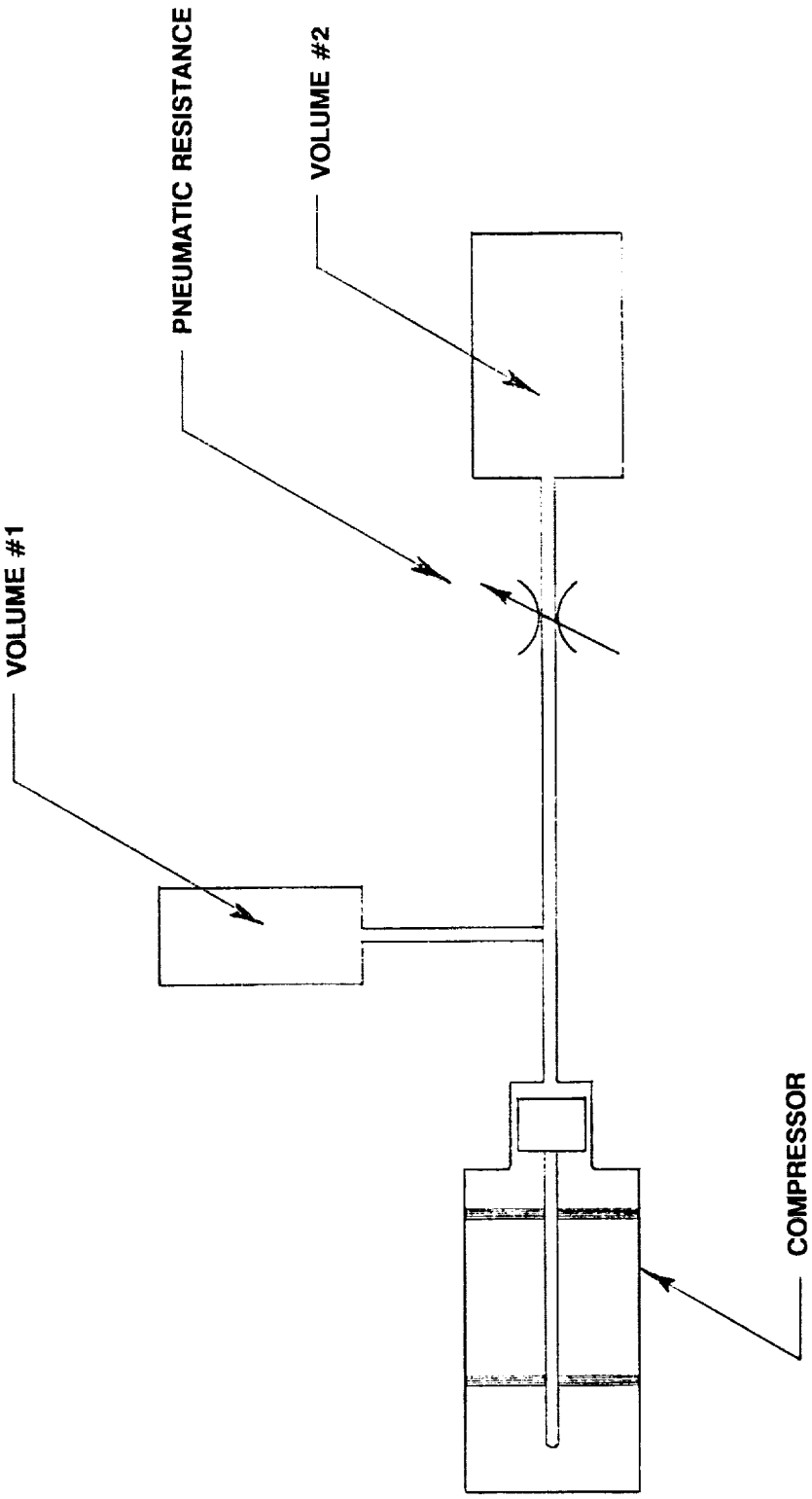

Figure 3. Pneumatic Circuit

adjusting the size of volume #1 until the velocity of the armature was in phase with the magnetic force.

The electric circuit is shown in Figure 4. The DC offset current, required to center the piston was measured using an inductor in series with a current meter. A capacitor in parallel with these two devices allows the AC component of the current to pass while blocking the DC component. The electrical input power to the motor was measured using a wattmeter. The compressor output power was calculated by measuring the PV work per cycle on an oscilloscope and multiplying by the frequency.

2.2.2 Efficiency

The overall efficiency of the compressor can be expressed as

$$\eta = 100\ (f \int PdV)/P_{in}$$

Figure 5 shows a pressure volume diagram at the design point, from which the output power can be calculated. The efficiency of the research compressor is 58.1% at the design point of 20 watts output power. The highest efficiency recorded was 64.2% with a power output of 28.2 watts. A plot of efficiency versus input power is shown in Figure 6. The plot shows that the efficiency of the compressor is dependent on input power and that there is an optimum value for the input power.

2.2.3 Axial Centering

When the compressor was running at the design point, the piston required a centering force of about 1.8 pounds. The center of the stroke tended to move toward the compression space if no centering force was applied. The centering force was applied to the motor armature by superimposing a D.C. offset current on the A.C. drive current. The D.C. offset current at the design point was about 0.75 amperes. The D.C. offset current is proportional to the centering force. The centering force depends partly on the pressure amplitude. A plot of centering force versus pressure amplitude is shown in Figure 7. The scatter in the data is probably due to random experimental error and temperature variation. It shows that about 0.8 pounds of the centering force is due to some effect other than the pressure amplitude.

4.0 Discussion and Conclusions

4.1 Possible Causes for Axial Decentering

From the experimental data, the axial decentering force can be quantified in terms of magnitude and direction. Part of the force is due to the change in pressure and part of the force is due to other causes. The specific causes and their quantities can't be determined from the experimental tests that have been done. The funding of the program was used up before we were able to investigate all of the causes of axial decentering.

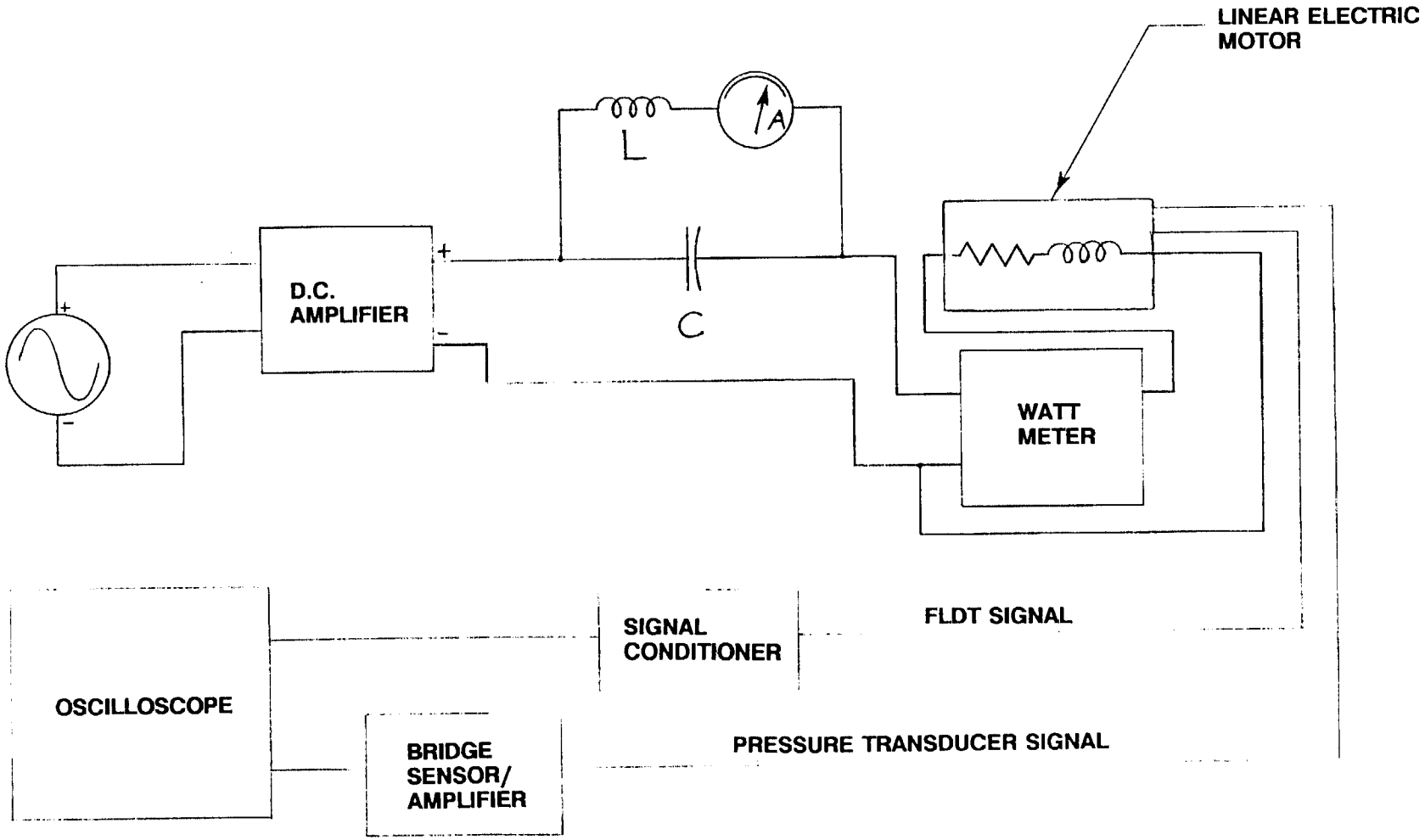

Figure 4. Electric Drive Circuit and Instrumentation

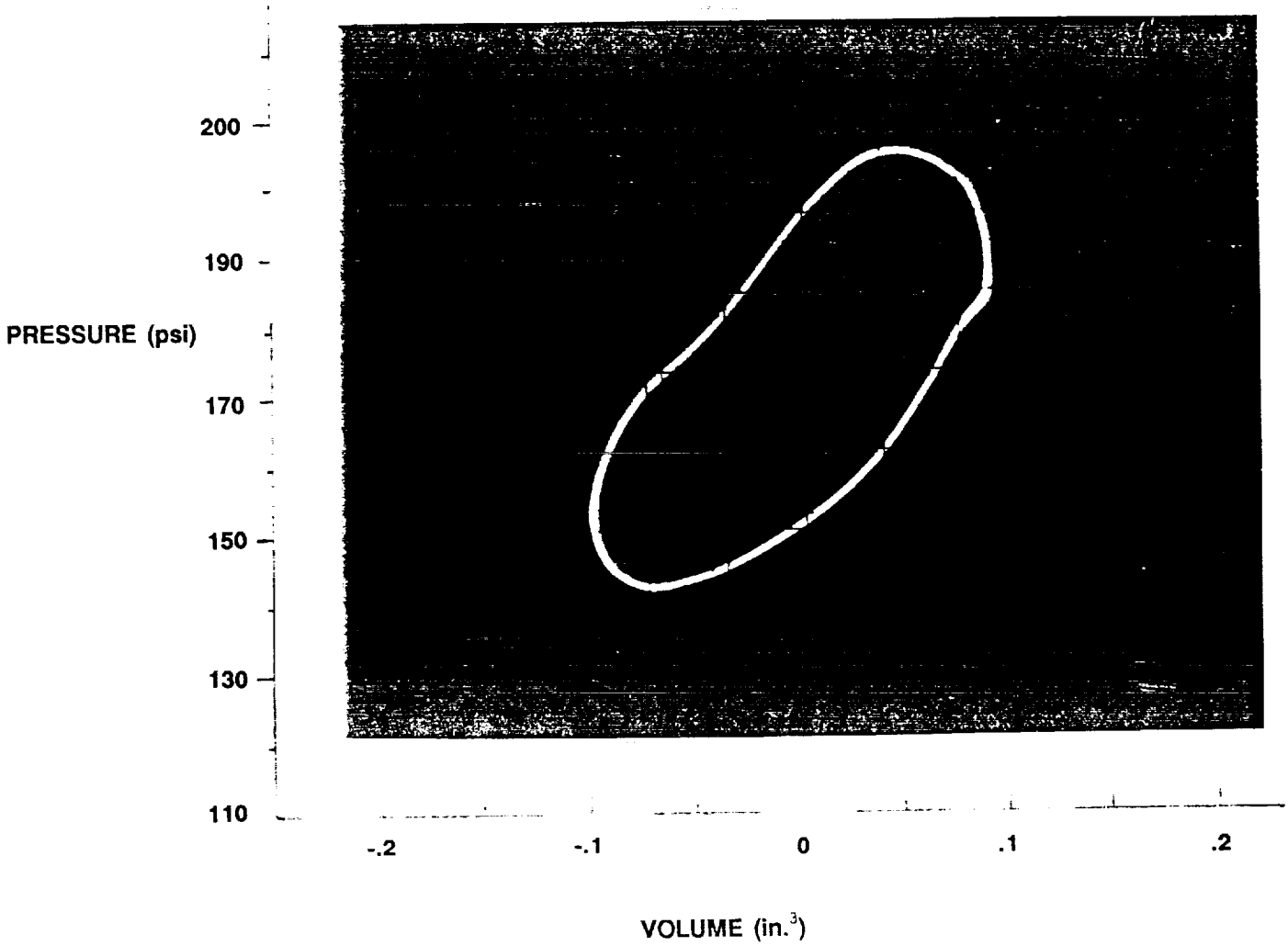

Figure 5. Oscilloscope Trace of a Pressure-Volume Diagram Representing 20 Watts of Power Output

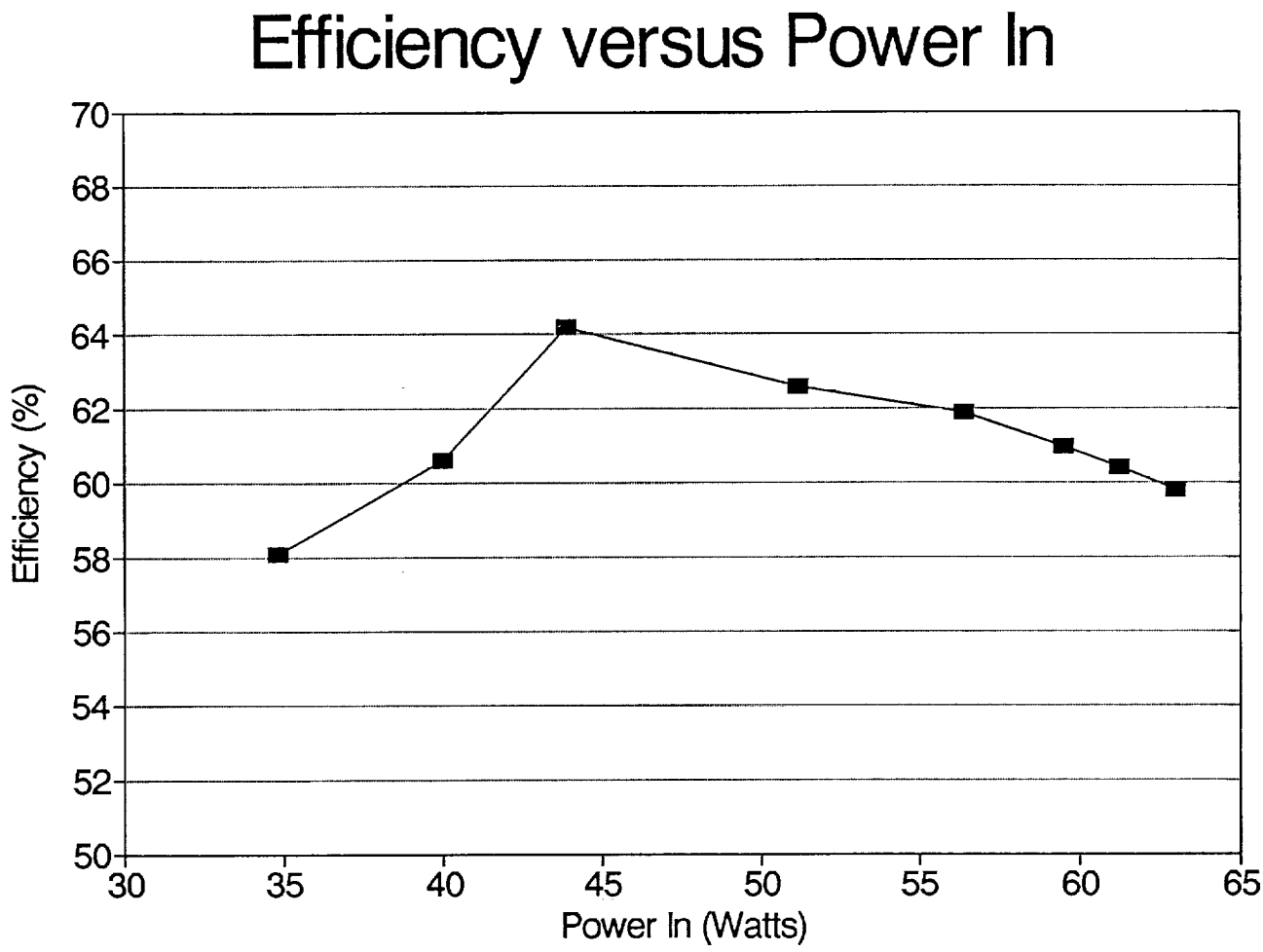

Figure 6. Compressor Efficiency Versus Input Power

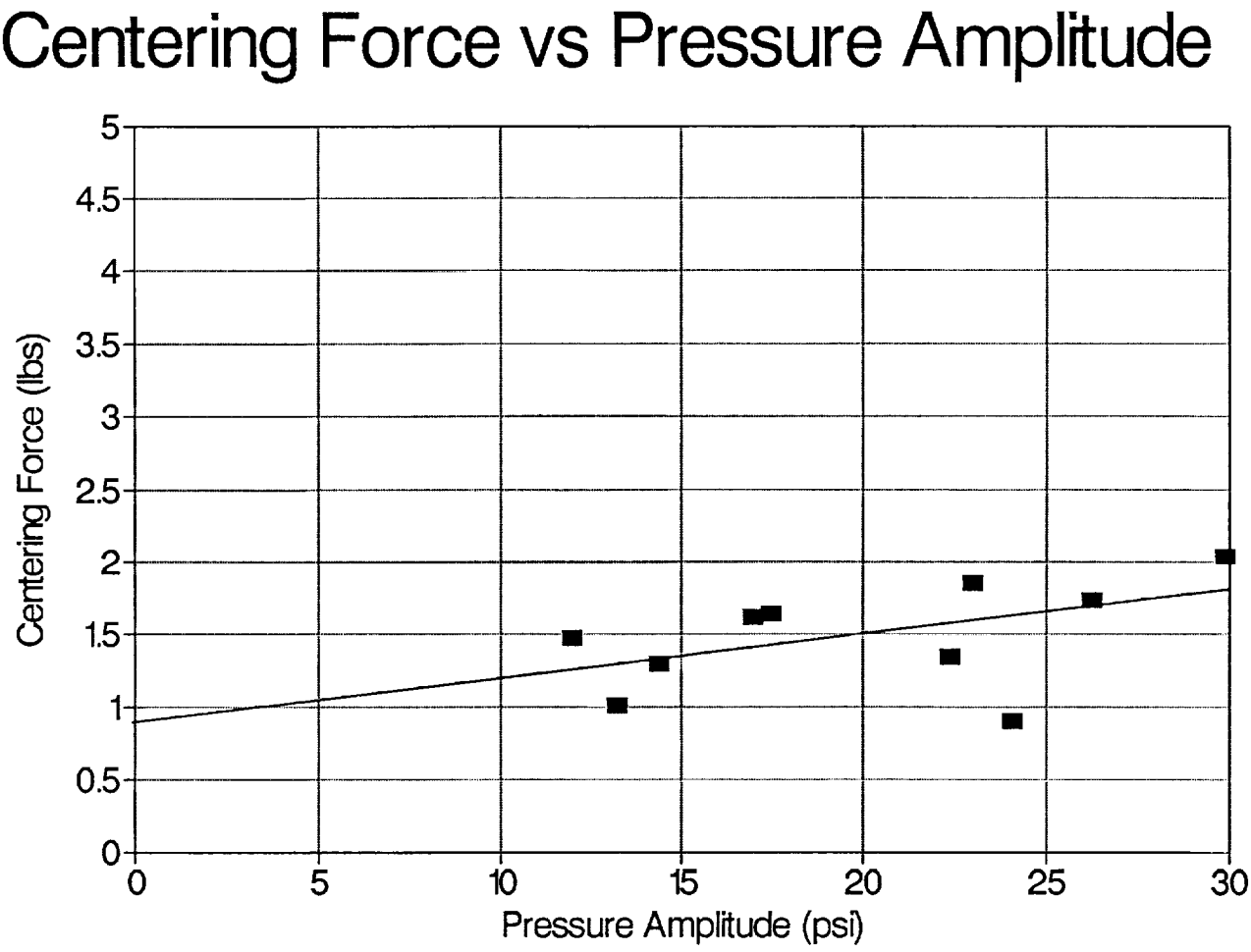

Figure 7. Armature Centering Force Versus Peak Pressure Amplitude

APPENDIX A

SEMI-ANNUAL REPORT
INVESTIGATION OF AXIAL POSITIONING FOR FLEXURAL COMPRESSORS

ORIGINAL PAGE IS
OF POOR QUALITY

SEMI-ANNUAL REPORT

INVESTIGATION OF AXIAL POSITIONING FOR FLEXURAL COMPRESSORS

Period Covered: 1 December 1988 - 14 December 1989

Grant NAG 5-1038

14 December 1989

Peter Riggle
Principal Investigator

TRI-CITIES UNIVERSITY CENTER
UNIVERSITY OF WASHINGTON
100 Sprout Road
Richland, WA 99352

Prepared for NASA GODDARD SPACE FLIGHT CENTER, Greenbelt, MD 20771

1.0 INTRODUCTION

This is a semi-annual report on NASA Grant NAG 5-1038. The research performed under this grant can be divided into flexural bearing research, which was conducted under the original grant, and research into axial positioning of the armature in cryocooler compressors employing flexural bearings, performed under an extension to the original grant.

2.0 SUMMARY

Summary of Flexural Bearing Research

Flexure research work funded by the original grant has been completed. Flexural bearings suitable for Stirling cryocooler applications have been demonstrated to provide long life at the desired stroke without failure or change in mechanical behavior. Tests have been conducted beyond 10^8 cycles room temperature and beyond 10^7 cycles at liquid nitrogen temperature. Structural analysis of flexures using the ANSYS finite element program has led to flexure shape improvements allowing a higher product of stroke and frequency than earlier designs. In addition, mechanical properties such as radial and axial stiffness, stress versus deflection, and modal frequencies have been established for specific flexure shapes and correlated with dimensional and physical parameters.

Summary of Armature Axial Positioning Research

The grant extension is intended to investigate means for axial positioning of armatures to prevent drift of the mean compressor piston position or of the compressor piston position at the end of the compression stroke. The research objective of the work is to characterize the axial force and electrical power required to position flexurally supported compressor pistons and armature assemblies. The axial positioning force is to be determined experimentally and will be theoretically related to a cyclic inconsistency in radial centering. The work to be performed under this grant extension includes the design and fabrication of a laboratory compressor module, measurements of centering current, and data reduction to interpret the current in terms of cyclic variation of piston radial eccentricity.

Excellent progress has been made. The design, fabrication, and assembly of the laboratory compressor module has been completed. The compressor has accumulated 10 hours of operating time. Initial testing has proven that DC bias can overcome

drift of the mean compressor position due to both gravitational forces and preferential gas migration.

Grant Extension Financial Status

Review of expenditures indicates about $10,000 remaining to be expended out of the grant extension total of $52,207. At the projected rate of expenditure, this will carry the research activity through to the scheduled conclusion of the project on 14 May 1990. At the current rate of progress, the proposed tasks will be completed within the time and funding provided.

3.0 RESEARCH PROGRESS

3.1 Flexural Bearing Research Progress

The bulk of the research work on flexural bearings for cryocooler applications was reported in a substantial mid-term report dated 20 December 1988. In the flexural bearing research work performed, the theory of flexural bearings was applied to select a flexure material and configuration for a 65 K cryocooler and to optimize the flexure. A test apparatus was designed and fabricated to test the flexure at room temperature and 80 K. Flexures were fabricated and tested through 10^8 cycles at room temperature and 10^7 cycles at 80 K.

A photograph of the overall test apparatus for the room temperature flexure tests is shown in Figure 1. The flexures are set up as bearings for a vertical rod, fastened into a rigid frame, and oscillated by shaking the frame vertically at the resonant frequency of the rod as suspended by the flexures. The damping of the rod/flexure combination is so low that the rod oscillates axially about 1 cm when driven about 0.003 cm. In the photograph, the motion of the flexure is being observed in slow motion by the use of a stroboscope. This allows verification that the mode shape of the flexure is well behaved, essentially the same as at very low frequency motion at the same amplitude. The position of the rod is measured using a linear displacement transducer. The position trace can be seen on the oscilloscope.

A photograph of one flexure of the group tested is shown in Figure 2. An improved flexure shape with about 50% improvement in stroke-frequency product was also developed under the original grant funding. The improved flexure shape,

ORIGINAL PAGE
BLACK AND WHITE PHOTOGRAPH

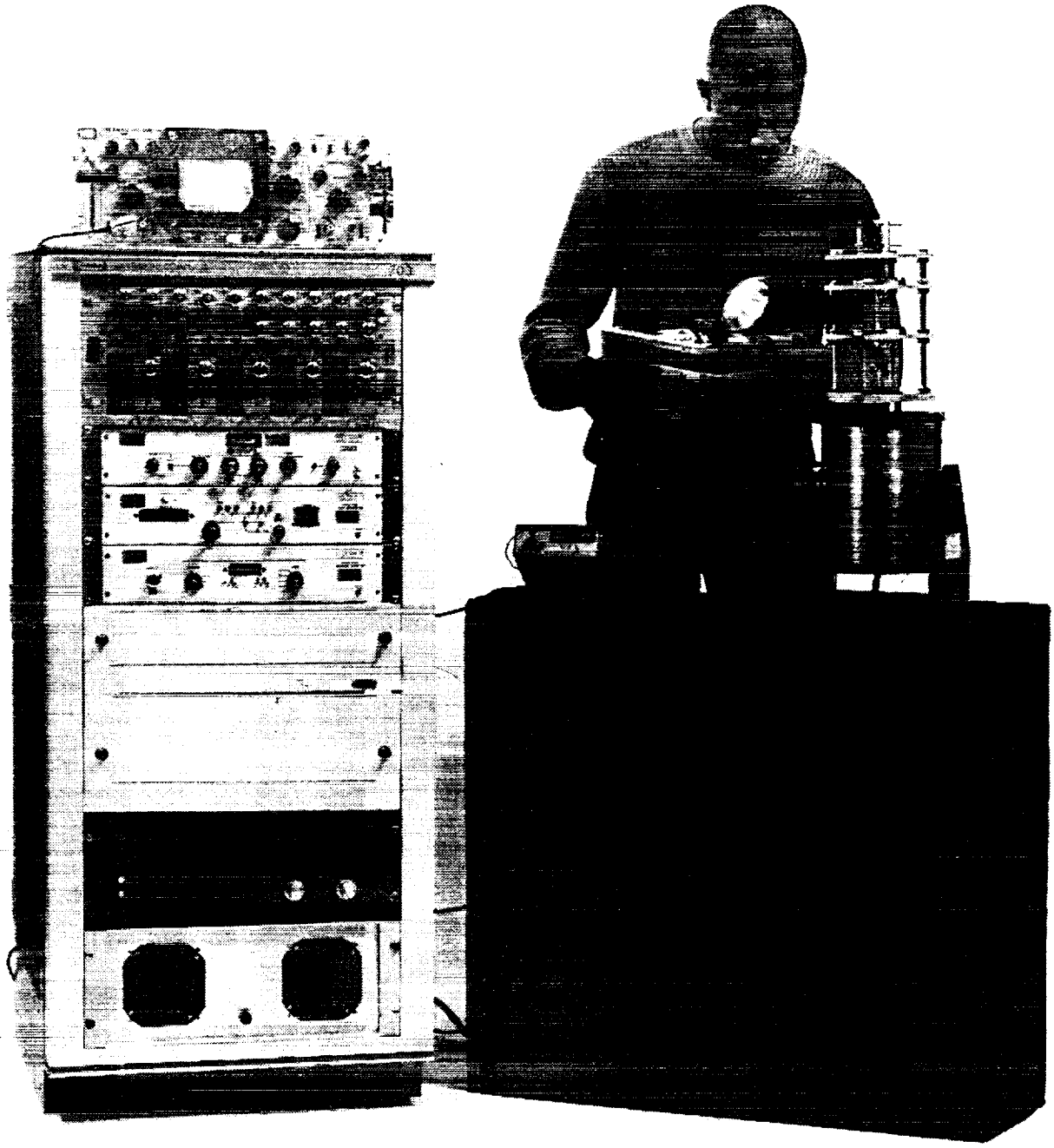

Figure 1. Flexure Test Apparatus

ORIGINAL PAGE
BLACK AND WHITE PHOTOGRAPH

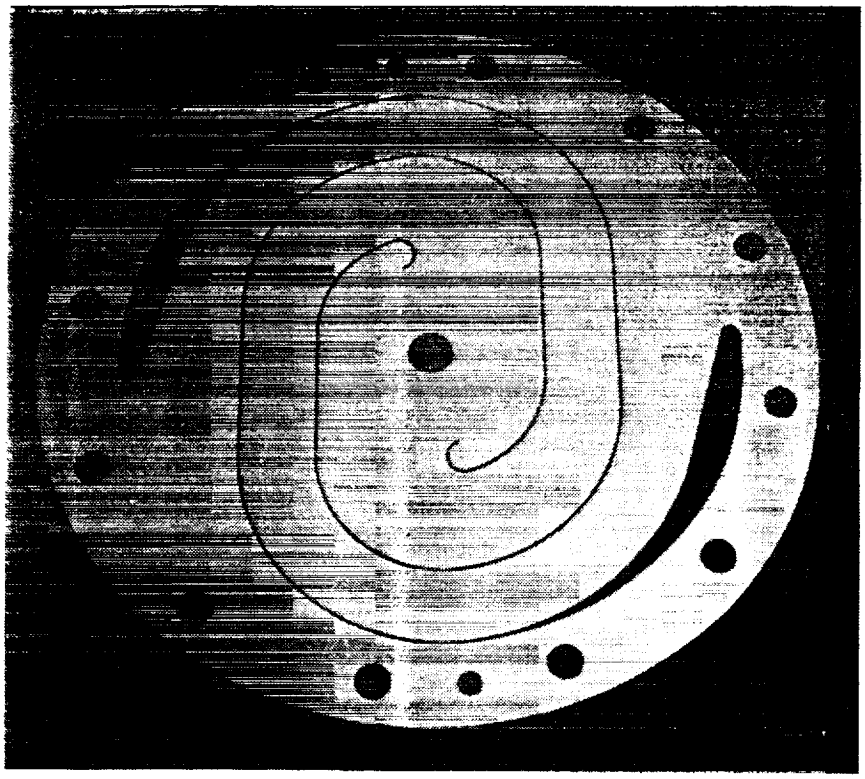

Figure 2. Beryllium Copper Flexure Tested Under NASA Goddard Grant

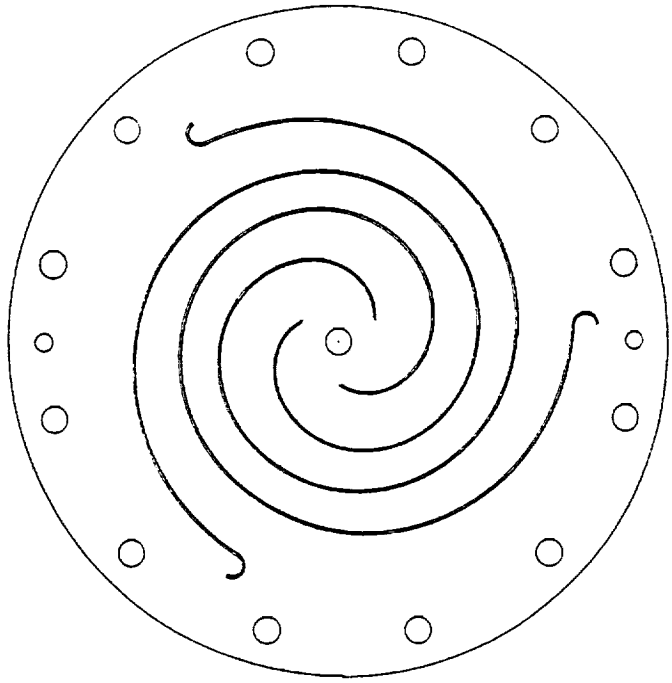

Figure 3. Improved Flexure Shape Developed Under NASA Goddard Grant

shown in Figure 3, is in use in the research compressor under development to investigate axial positioning effects.

Figure 4 is a closeup photograph of the flexures on test. Although this photograph was taken with the test stopped and the flexure artificially extended, the resulting image looks just as it would if viewed with the stroboscope.

STC is currently running the flexure test apparatus to obtain further fatigue data on flexures and is simultaneously using the apparatus to life test a flexible electrical lead configuration used on the research compressor under development as part of the grant extension.

We have concluded from finite element method results that the normalized equivalent stress distribution for a given flexure planform is independent of the thickness for the ratios of thickness to diameter of interest. This leads us to believe that the optimal planform shape of a flexure with a given arm length to width ratio is independent of thickness in the thickness range of interest.

It is worth noting here that the use of finite element analysis is an improvement over the experimental methods we have employed in the past to refine flexure shape. In addition to conveniently providing detailed information on spring rates and mode shapes and frequencies, the finite element method pinpoints the small areas of very high stress near flexure arm end terminations much more precisely then can be done experimentally.

Analytical work completed as part of the flexural bearing research is summarized in Table 1.

3.2 Axial Positioning Research Progress

Progress of the axial positioning research is discussed in this section in a task oriented format. Progress has followed the objectives as outlined in the proposal statement of work.

ORIGINAL PAGE
BLACK AND WHITE PHOTOGRAPH

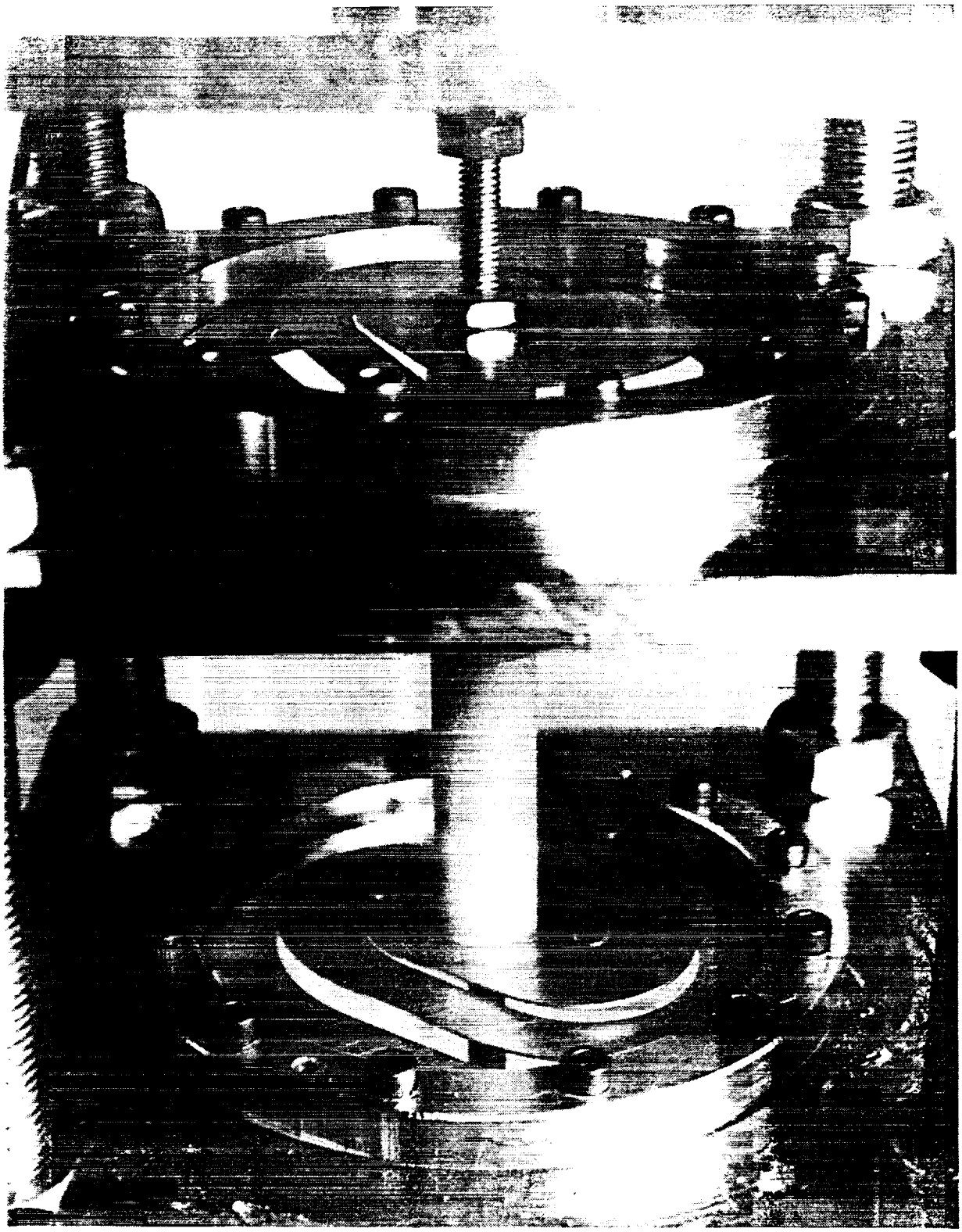

Figure 4. Closeup of Flexures on Test

Table 1

COMPLETED ANALYTICAL WORK

1. Flexure material figure of merit survey (best allowable stroke/frequency product).
2. Axial and radial spring rates, radial spring rate when flat, radial spring rate when axially deflected, and the effect of direction upon radial spring rate.
3. Peak principal stresses versus deflection.
4. Peak equivalent stresses versus deflection.
5. Effect of thickness upon stress.
6. Flexure shape revision for lower peak stress.
7. Flexure arm mode shapes and modal frequencies.
8. Projections of allowable flexure stroke and frequency for various diameters and thicknesses.
9. Selection of flexural bearing parameters for the research cryocooler.

3.2.1 Task 1 - Design, fabricate and assemble a laboratory flexural compressor. To minimize development risk, the research compressor was designed along lines similar to a published layout for the Oxford ISAMS flight cooler. Design simplifications were incorporated where possible to reduce cost. The layout can be seen in Figure 5. The flexure planform shape selected for the research compressor was based upon flexure research discussed earlier.

Analyses were performed during the design of the laboratory compressor to evaluate the compressor driving an 80 K expander and, alternatively, driving a pneumatic resistance for axial positioning research. Analyses included: 1) design of the motor, 2) dynamic and electrodynamic analyses of a cryocooler incorporating the compressor, and 3) dynamic and electrodynamic analyses of the compressor driving a pneumatic resistance.

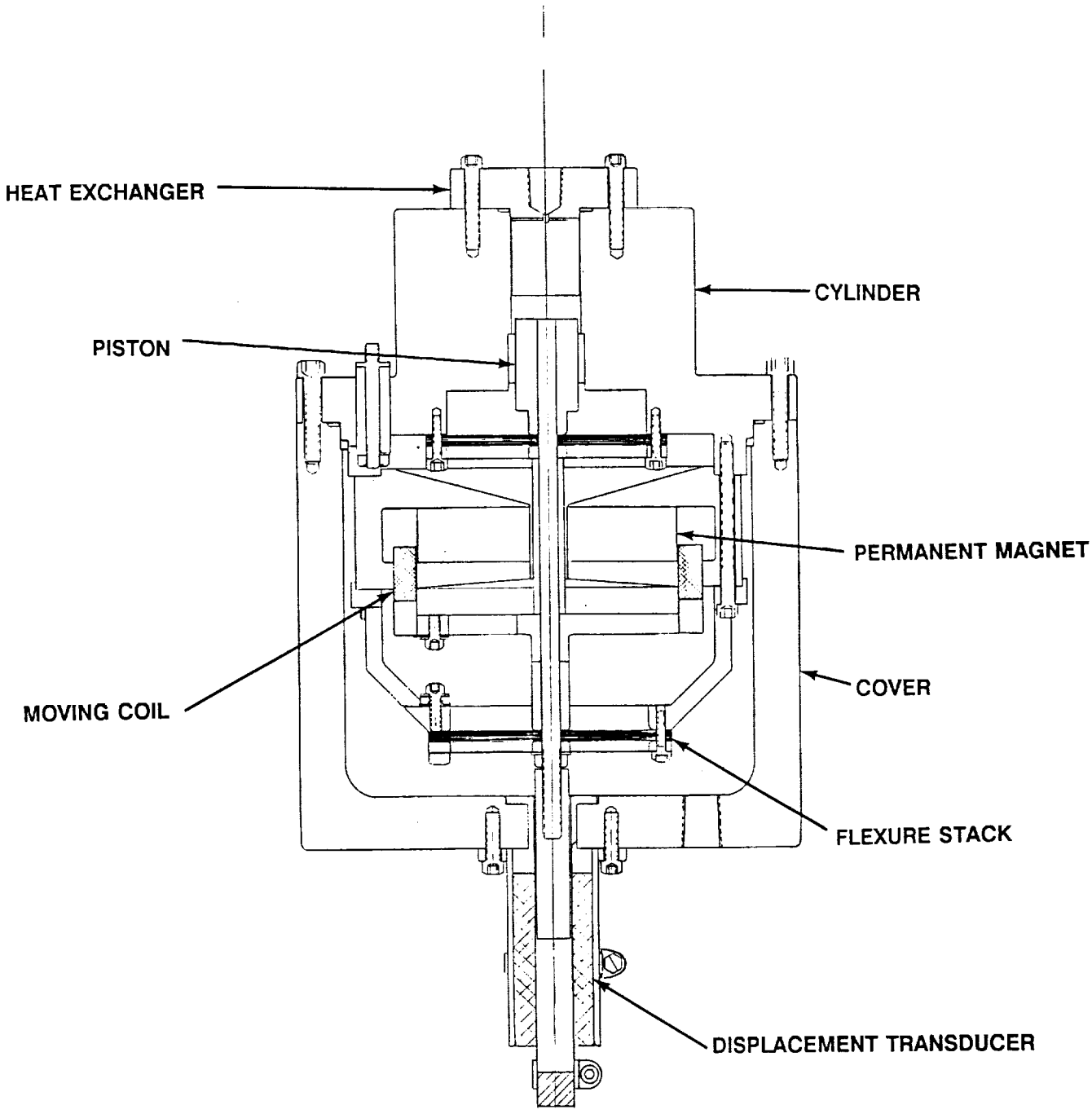

Figure 5. Engineering Layout of Research Compressor

Magnetic Circuit Analysis

Closed form algebraic equations were used to analyze the motor magnetic circuit using an equivalent electrical circuit analogy. This analysis resulted in the specification of the magnet and included a calculation for both the expected magnetic field strength and the motor coil packing factor. Measurements of the field strength and the packing factor correlated well with calculated values.

Analysis of the Research Compressor Driving a Cryocooler

Dynamic and electrodynamic analyses were performed to develop research compressor parameters which make the compressor suitable for use in a Stirling cycle cryocooler. The results of these analyses were incorporated into the design of the laboratory compressor. Two alternative analyses methods were used, an impedance analysis and a dynamic system simulation. The two methods produced comparable results. The dynamic simulation provides less overall insight, but allows the non-linearity of the working gas to be considered.

Impedance analysis of the cryocooler shows that the highest motor efficiency occurs when the inertial reactance of the armature is perfectly balanced by an opposed stiffness of the flexural bearings combined with the pneumatic stiffness of the working gas acting on the compressor piston. When these reactances are balanced, the remaining mechanical load is the pure mechanical resistance of the working gas acting on the compressor piston and the mechanical impedance angle is zero.

The effect of the mechanical impedance angle on motor efficiency of the research compressor is presented in Figure 6. The research laboratory compressor has an impedance angle of approximately -20 degrees. Increasing the mass of the motor armature would decrease the magnitude of the impedance angle which in turn would increase the efficiency. However, the armature mass would have to double to approach zero impedance angle.

Clearance Seal Losses

Figure 7 establishes the relationship between compressor radial clearance and the losses associated with gas leakage past the piston clearance seal. The curve is based upon a mean pressure of 1.2 MPa and a pressure amplitude of 0.234 MPa. The laboratory compressor was designed with a compressor radial

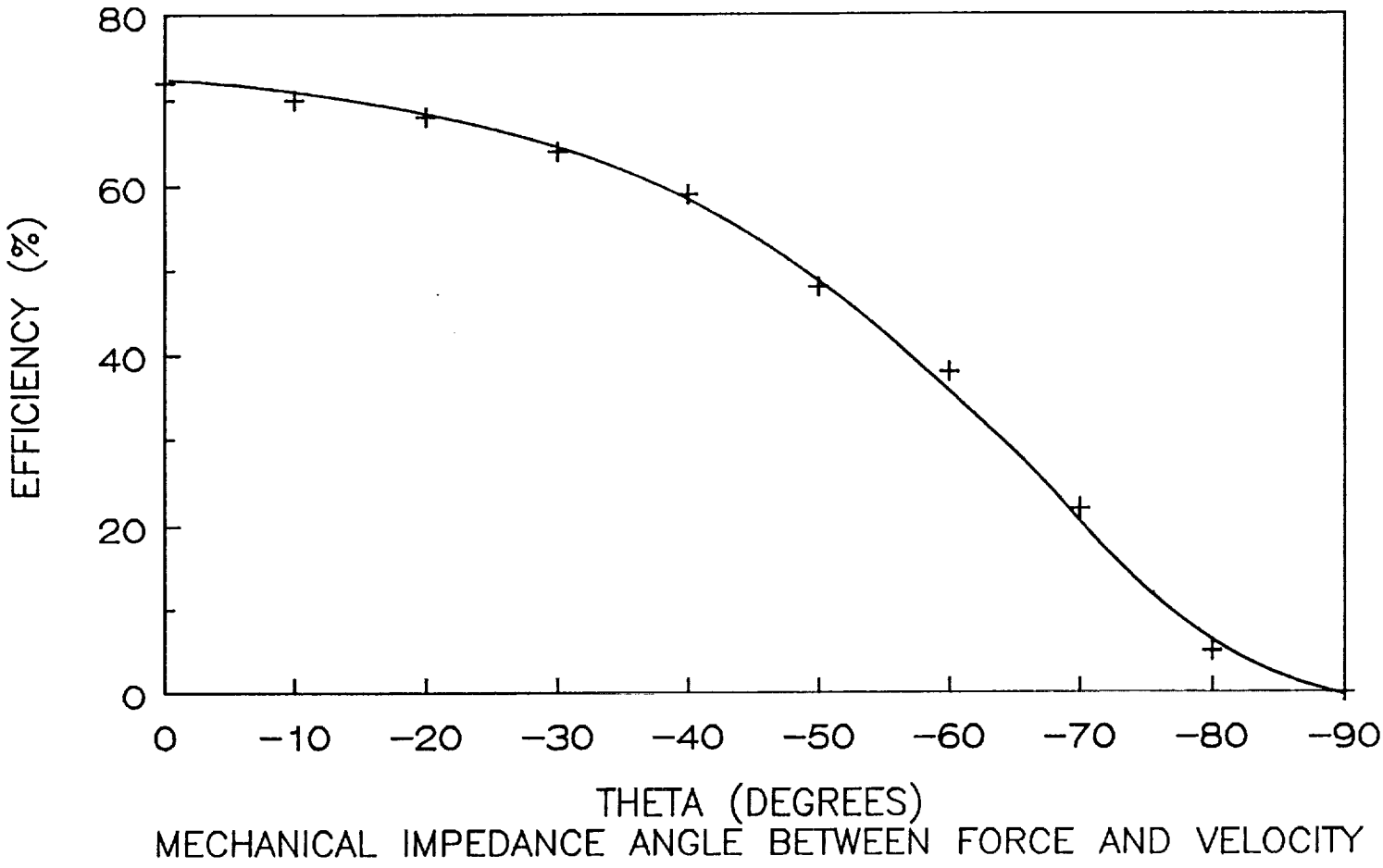

Figure 6. Efficiency vs. Mechanical Impedance Angle

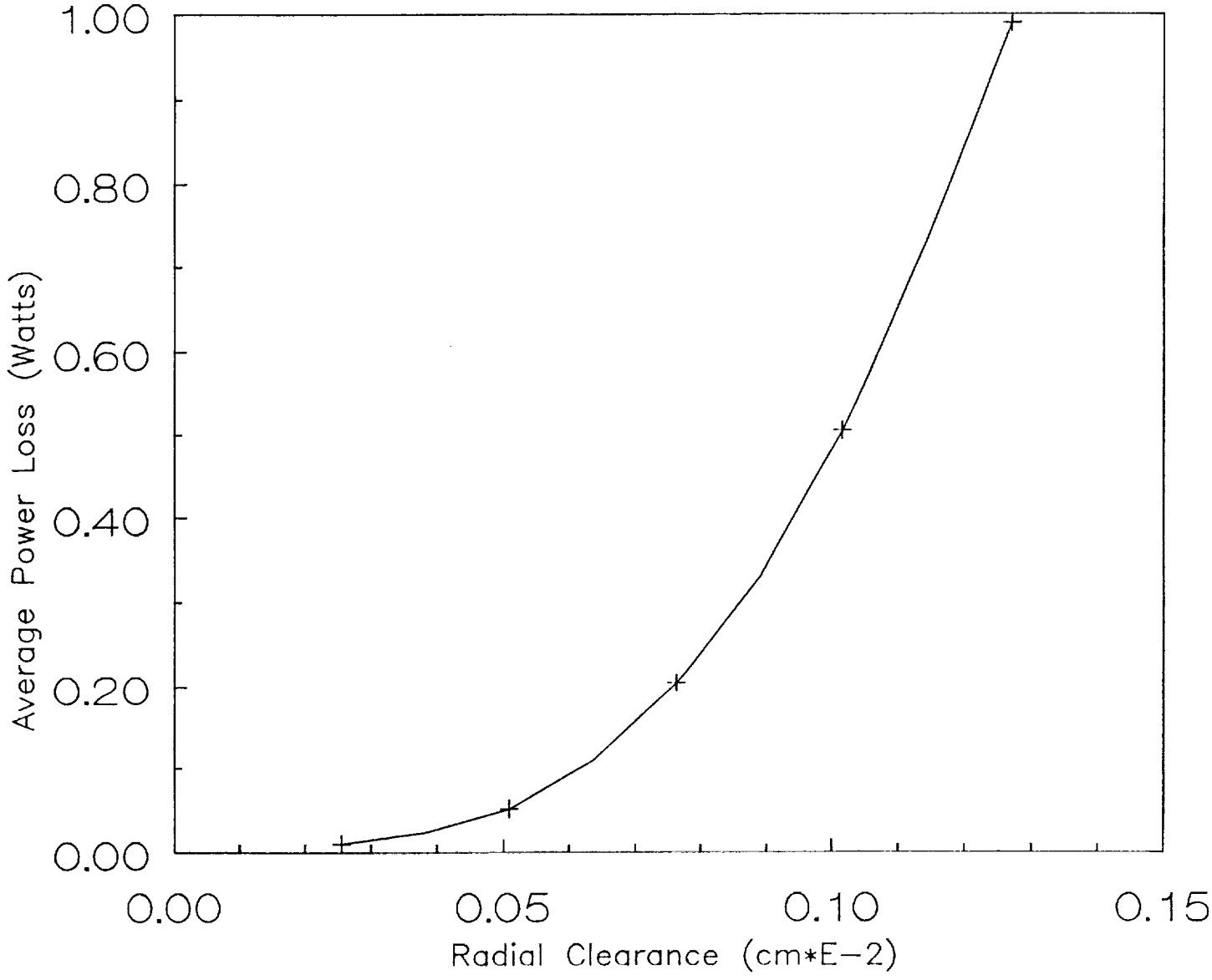

Figure 7. Average Power Loss vs. Radial Clearance

clearance of 7.62×10^{-3} mm. The associated losses are limited to 0.2 watts with that clearance.

The Research Compressor Driving a Pneumatic Resistance

A schematic of the research compressor test load is shown in Figure 8. Impedance analysis has been carried out for the research compressor driving a pneumatic resistance at 40 Hz with a 1 cm stroke at 1.2 MPa mean pressure. Impedance analysis was used to select a reservoir volume for the test load. The reservoir and the pneumatic resistance were adjusted in the analysis to obtain a condition providing: 1) 20 watts pneumatic power dissipation in the resistance at 1 cm stroke and 40 Hz, and 2) pneumatic stiffness sufficient to resonate the moving mass of the armature assembly. A curve of calculated pneumatic power dissipation versus valve resistance is presented in Figure 9. Experiments to date have established the capacity of the test load to dissipate up to 30 watts of pneumatic power by varying the pneumatic resistance. Power dissipation in the pneumatic resistance is the only significant load upon the electrical motor.

Mechanical Design

In the mechanical design of the research compressor, emphasis was placed upon the details that affect the ability of the piston/armature assembly to run without rubbing between the piston and the cylinder. A study was carried out to establish the tolerances on component geometry to prevent rubbing. The resulting tolerances were specified on the detailed engineering drawings of the components requiring dimensional control. All structures affecting alignment of the piston within the cylinder were designed as bodies of revolution to minimize effects of temperature and pressure changes upon alignment of the piston within the cylinder.

The engineering layout for the research compressor was presented earlier in Figure 5. The piston and cylinder, the cover, and several other structural components are machined from 6061-T6 aluminum alloy. Figure 10 shows the completed motor coil. Figure 11 shows the compressor without the cover. Figure 12 shows the compressor operating on its test stand. This photograph shows the power leads, the pressure transducer leads and the tubing from the compressor on the bottom. The displacer transducer and the tubing from the motor

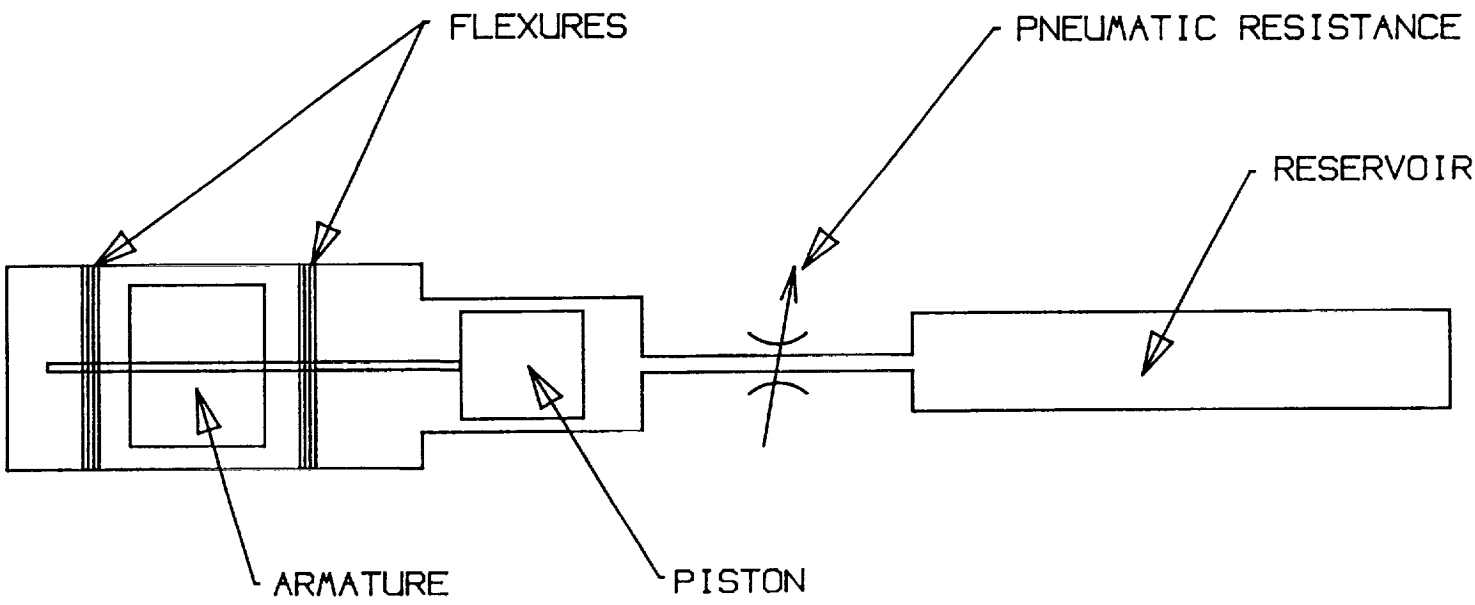

Figure 8. Schematic for Research Compressor Test Apparatus

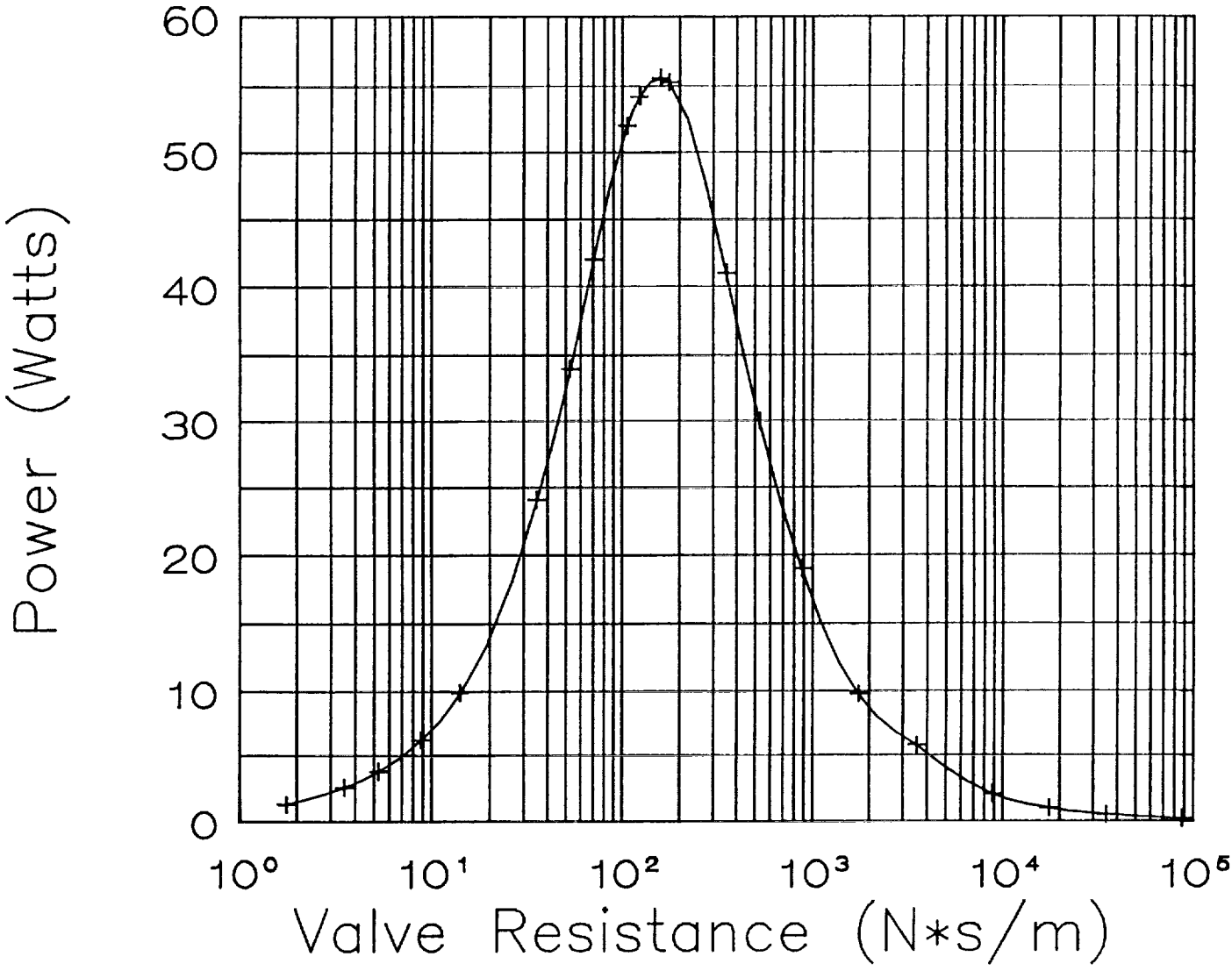

Figure 9. Motor Power vs. Valve Resistance

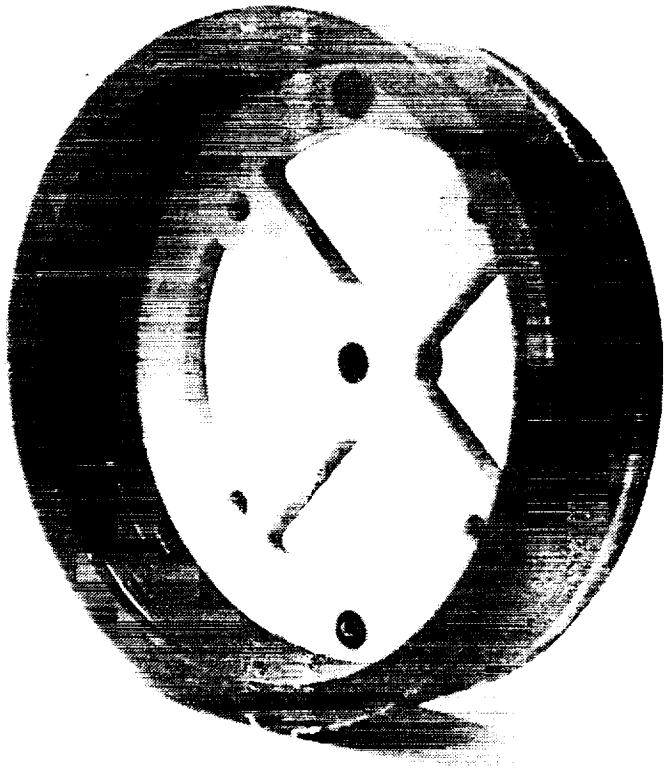

Figure 10. Motor Coil

ORIGINAL PAGE
BLACK AND WHITE PHOTOGRAPH

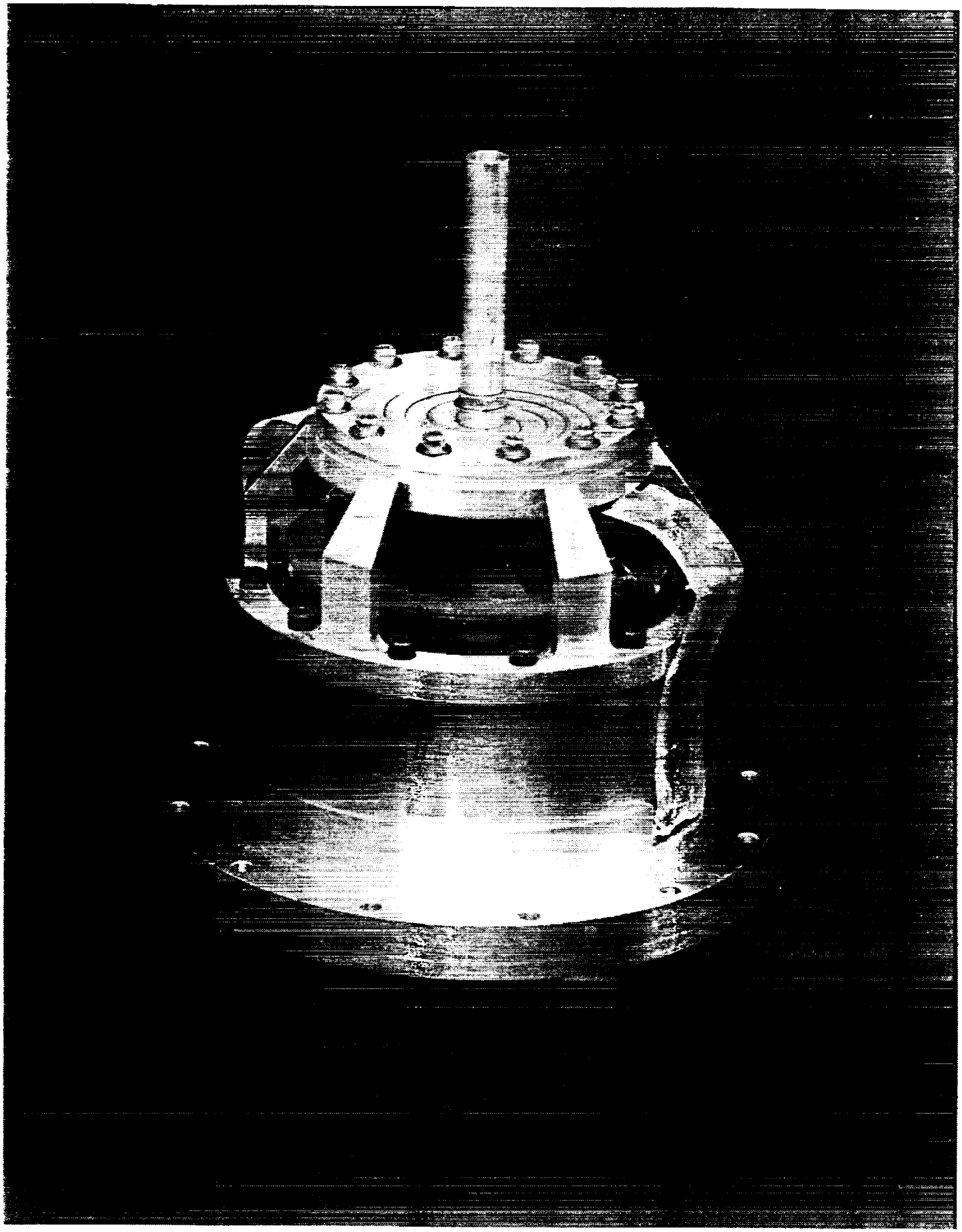

Figure 11. Research Compressor

ORIGINAL PAGE
BLACK AND WHITE PHOTOGRAPH

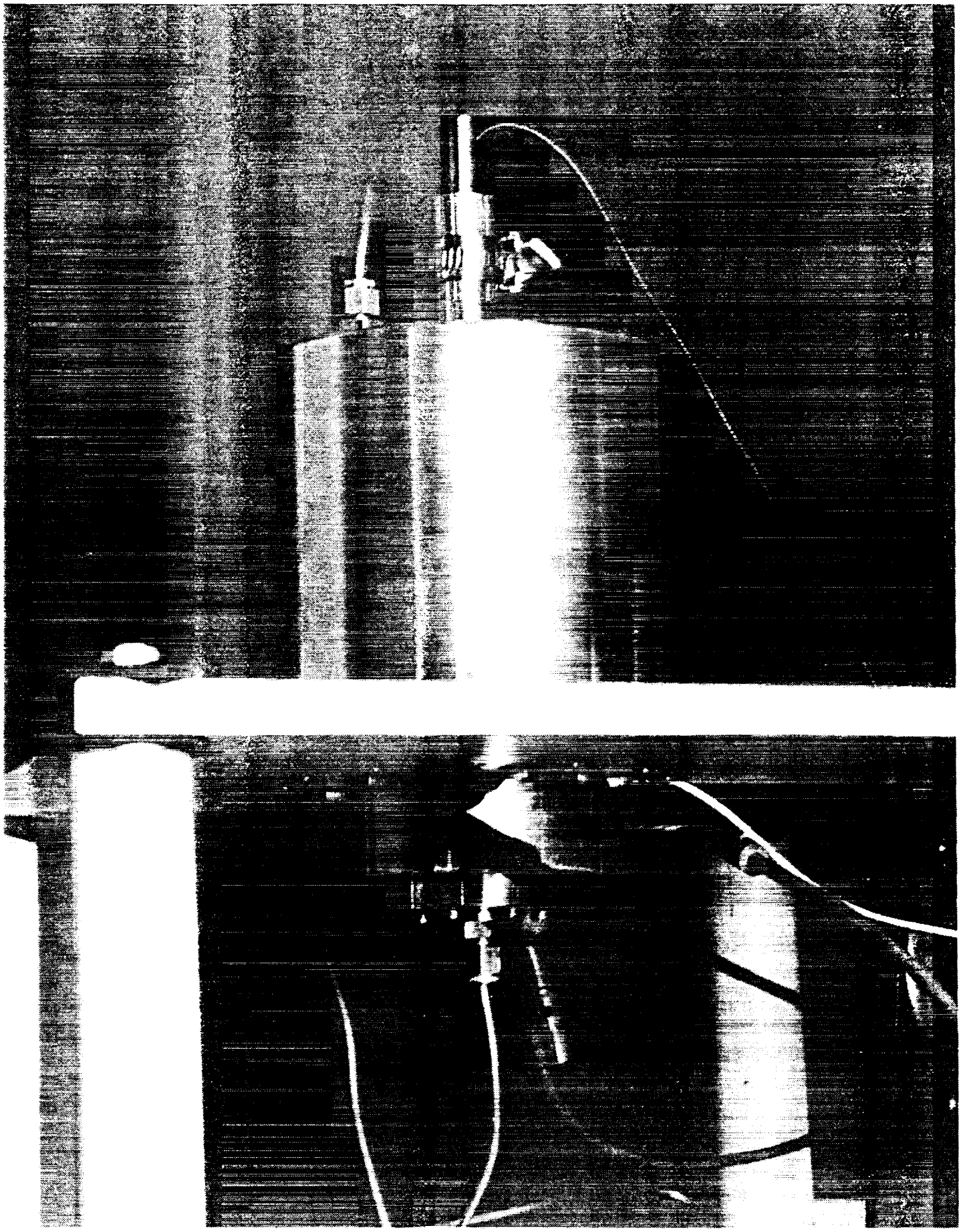

Figure 12. Research Compressor Under Test

ORIGINAL PAGE
BLACK AND WHITE PHOTOGRAPH

volume are shown at the top. The compressor has now accumulated 10 hours of problem-free operation.

A new plexiglas cover has just been completed and installed. This allows the flexures to be observed using a stroboscope while the compressor is operating at the design point. Photographs will be included in the final report. The purpose of the plexiglass cover is to detect any unwanted modal vibrations of the flexure arms, should they occur.

3.2.2 Task 2 - Perform tests to determine the force required to position the compressor pistons and the electric current and power dissipation corresponding to the positioning force. Disassemble, reassemble, and test repeatedly to obtain data on the random variability to be expected in the axial centering force.

This task is just getting underway. The equipment necessary to perform the task has been assembled and can be seen in Figures 13 and 14. PV work can be seen in the lower oscilloscope trace (pressure and volume are shown on the horizontal and vertical axes, respectively). The upper oscilloscope traces are the drive voltage and current.

3.2.3 Task 3 - Develop an analytical model which interprets the experimentally determined positioning force as a variability of compressor piston eccentricity within each cycle. Reduce the data.

This task is not yet underway.

3.2.4 Task 4 - Provide one mid-term research report and one final research report.

This report serves as the mid-term research report. The final report will be sent at the conclusion of this project, on or before 14 May 1990.

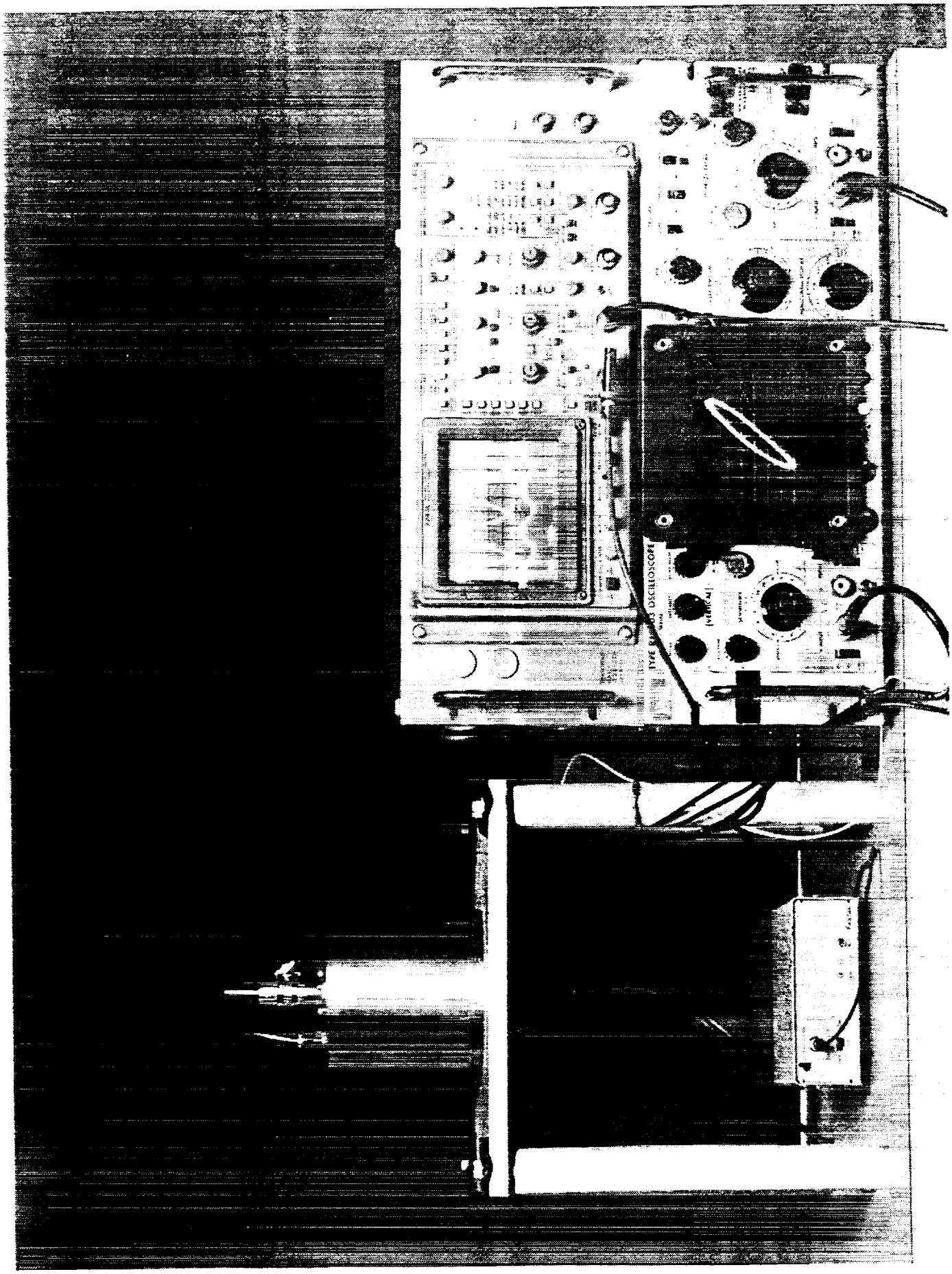

Figure 13. Compressor Test Stand

ORIGINAL PAGE
BLACK AND WHITE PHOTOGRAPH

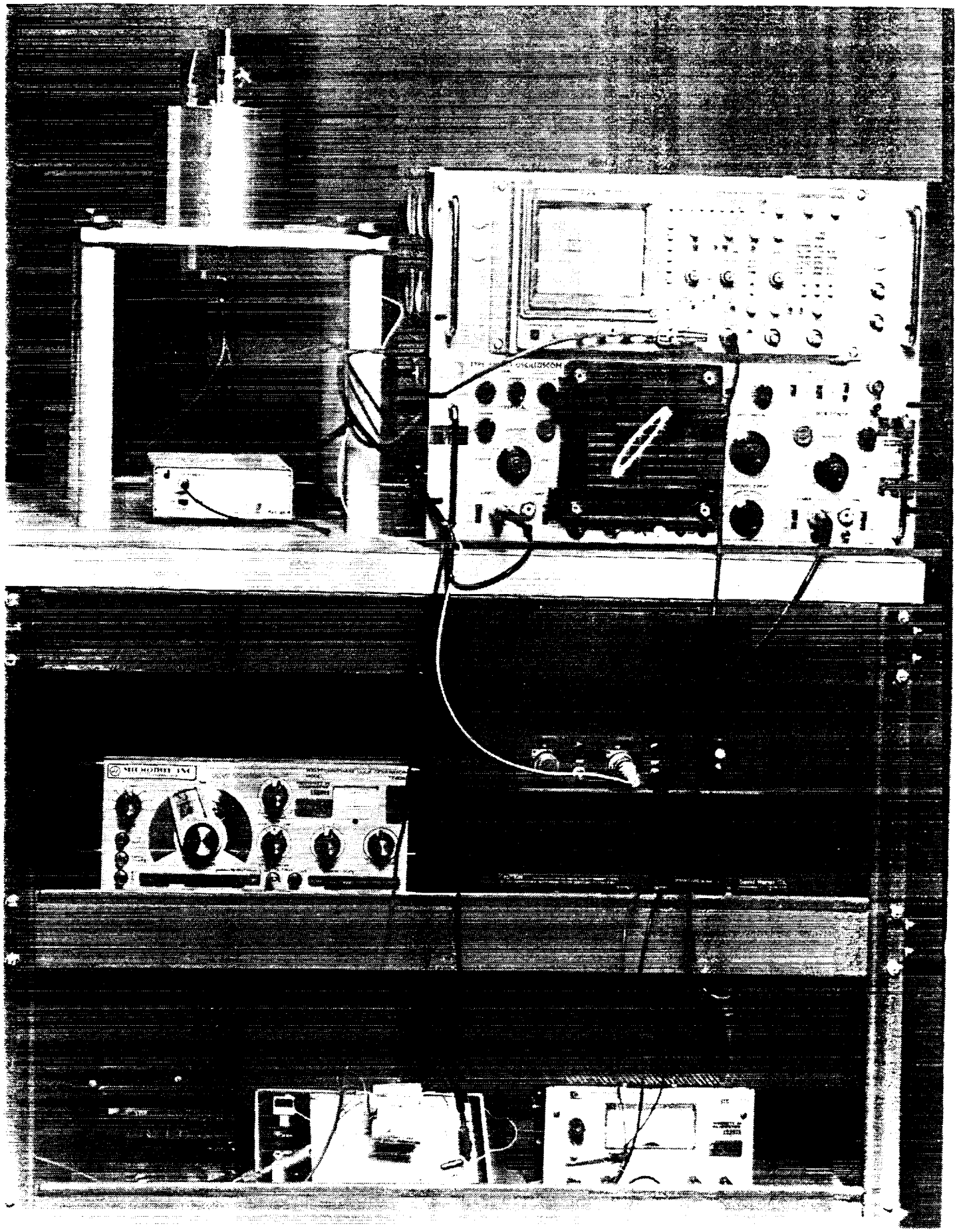

Figure 14. Compressor Test Stand

ORIGINAL PAGE
BLACK AND WHITE PHOTOGRAPH